2012 American Control Conference
Fairmont Queen Elizabeth, Montréal, Canada
June 27-June 29, 2012

Nonlinear Modeling of a Miniature Fixed-Pitch Coaxial UAV

Fei Wang, Swee King Phang, Jinqiang Cui, Guowei Cai, Ben M. Chen, Tong H. Lee

Abstract— **This paper presents the work that has been done to derive an accurate nonlinear model for a miniature fixed-pitch coaxial helicopter. Starting from the Newton-Euler rigid body dynamic equations, forces and torques generated at various parts of the UAV have been identified and formulated. The physical meanings behind the model are clearly explained, and the methods of identifying all the important model parameters are also provided. The full model is verified by comparing simulation results and actual flight tests with the NUS FeiLion coaxial UAV. The agreement between the two is promising.**

Index Terms— **Nonlinear model, coaxial helicopter, micro unmanned aerial vehicle.**

I. Introduction

To date, the advancement in small yet sophisticated electronics such as microprocessors and MEMS-based sensors has driven the development of the unmanned aerial vehicle (UAV) to a brand-new era. Many researchers have changed their motivation from developing large outdoor UAVs to discovering the potential of miniature indoor UAVs. Interesting platforms, such as flapping-wing, coaxial and quad-rotor UAVs, have been constructed for indoor tasks due to their small size and adequate maneuverability.

In the past three years, the UAV research team from the National University of Singapore (NUS) has been developing miniature indoor UAVs by adopting the coaxial configuration. The coaxial configuration provides several advantages over the other types of platforms, summarized as follows:

1) It is relatively stable due to the damping effect introduced by a stabilizer bar [1];
2) It is proven to be more power efficient as compared to the single-rotor or quad-rotor configurations [2];
3) It has higher maximum forward speed than a single-rotor helicopter since it always has a pair of advancing and retreating blades, creating a symmetric lift in forward flight [3];
4) It has higher payload to dimension ratio than all the other configurations.

In order to achieve high-performance autonomous control, an efficient and robust feedback control law needs to be designed. This makes a precise model of the UAV indispensable. A comprehensive guide to identify the nonlinear model of miniature single-rotor helicopter has been described in the works by Mettler [4] and Cai *et al* [5]. There are, however, significant mechanical differences between the single-rotor and coaxial configurations, which make the described model inapplicable to the latter.

A major difference between the two is that the coaxial platform consists of two concentric rotors rotating in opposite directions, while both rotors must take into account of the induced velocity caused by one another. Such relationship is described in [6]. A detailed study of the wake dynamics of the two rotors is also documented in [7].

Another specialty of miniature coaxial helicopter is the stabilizer bar attached to the top rotor hub, which passively stabilizes the helicopter. It, however, causes strong influences to the rotor dynamics especially to the fixed-pitch coaxial configuration as the upper rotor is not linked to any servo. As a result, the cyclic pitch control of the upper rotor is solely induced by the stabilizer bar. The stabilizer bar dynamics is commonly modeled as a first order lag system [1]. In the works shown in [1] and [8], the tip-path-plane (TPP) dynamics is separated into the upper and lower portion, where only the lower TPP is controlled by the servo inputs.

In a few recent works on the modeling of miniature coaxial helicopter, although fairly complete nonlinear or linear models are obtained, the works lack intuitive explanation of the model formulation. Moreover, their methods of parameter identification are not comprehensive enough. For example in [9], the helicopter dynamics were treated as a black box, while the whole system is vaguely identified using the CIFER (Comprehensive Identification from FrEquency Responses) toolkit. To complement the existing work, this paper presents the detailed derivation of the nonlinear model for a fixed-pitch coaxial helicopter, together with experimental methods used to identify the key parameters of the model.

The content of this paper is organized as follows: Section II briefly describes the working principles of a fixed-pitch coaxial helicopter and provides an overview of the model structure. Next, Section III gives the detailed formulation of the nonlinear model of the platform, together with parameter identification methods. Section IV verifies the derived model by comparing simulation results with the actual flight test data. Lastly, concluding remarks based on all the presented work are made in Section V.

II. Basic Working Principle and Model Overview

A few miniature UAVs, codenamed PetiteLion [10], KingLion [11] and FeiLion [12] (see Fig. 1) have been developed by the NUS UAV research team for various indoor navigation projects. These UAVs adopt the Esky Lama series coaxial helicopters as their bare platforms. The nonlinear model derived in this paper is applicable to all these UAVs,

F. Wang, S. K. Phang and J. Cui are with the NUS Graduate School for Integrative Sciences & Engineering, National University of Singapore (NUS), Singapore. E-mail: {g0901899,a0033585,a0068416}@nus.edu.sg

G. Cai is with the Temasek Laboratories, NUS, Singapore. E-mail: tslcaig@nus.edu.sg

B. M. Chen and T. H. Lee are with the Department of Electrical & Computer Engineering, NUS, Singapore. E-mail: {bmchen,eleleeth}@nus.edu.sg

Fig. 1. From left to right: PetiteLion, KingLion, FeiLion

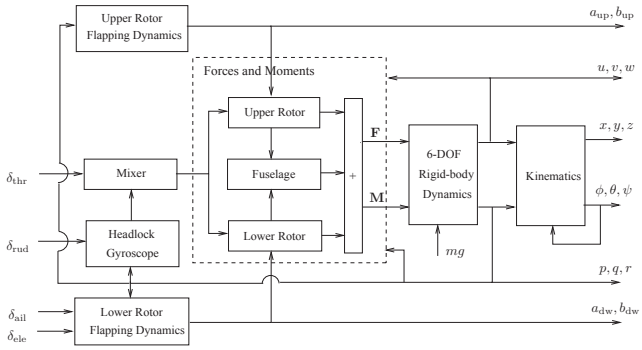

Fig. 2. Overview of model structure

while the parameters identified were based on the latest platform – FeiLion.

For a fixed-pitch coaxial helicopter, the collective pitch of the rotor blades cannot be changed. Heave and yaw motion of the helicopter can only be achieved by varying the rotational speed of the rotors, which are controlled by two separate motors. Generally, the summation of the motor speeds determines the helicopter vertical motion, while the difference of the two determines the yaw motion. Rolling and pitching are accomplished by introducing a slanted orientation of the swashplate, which is controlled by the aileron and elevator servos. In this way, a tilted flapping of the rotor blades can be induced, and the corresponding thrust generated becomes non-vertical.

An overview of the model structure is shown in Fig. 2. δ_{ail}, δ_{ele}, δ_{thr} and δ_{rud} are the aileron, elevator, throttle and rudder inputs to the whole system. State variables can be found at the right side of the figure. From the inputs to the state variables, there are numerous blocks representing all the sub-systems involved. In the next section of this paper, mechanisms in all these blocks will be explained in detail.

III. Model Formulation and Parameter Identification

A. Coordinate systems and rigid-body dynamics

As a common practice of aeronautic analysis, two main coordinate frames will be used in this paper. One is the North-East-Down (NED) frame and the other is the body frame. While the NED frame is stationary with respect to a static observer on the ground, the body frame is placed at the Center of Gravity (CG) of the coaxial helicopter, where its origin and orientation move together with the helicopter fuselage (see Fig. 3). To obtain the relationship between the NED-frame position and the body-frame velocity, one has

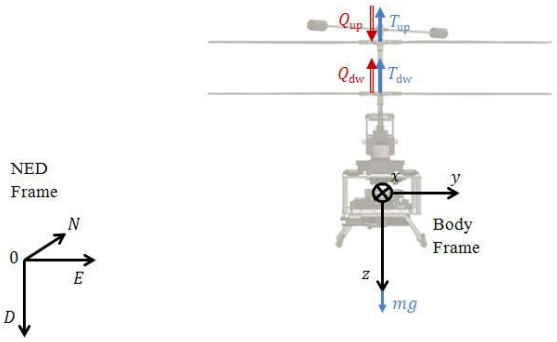

Fig. 3. Coordinate frames and various forces and torques

the following well-known navigation equation:

$$\begin{pmatrix}\dot{x}\\ \dot{y}\\ \dot{z}\end{pmatrix} = \begin{bmatrix} c_\psi c_\theta & c_\psi s_\theta s_\phi - s_\psi c_\phi & c_\psi s_\theta c_\phi + s_\psi s_\phi \\ s_\psi c_\theta & s_\psi s_\theta s_\phi + c_\psi c_\phi & s_\psi s_\theta c_\phi - c_\psi s_\phi \\ -s_\theta & c_\theta s_\phi & c_\theta c_\phi \end{bmatrix} \begin{pmatrix}u\\ v\\ w\end{pmatrix}, \tag{1}$$

where x, y, z are the NED-frame position components of the helicopter and u, v, w are the body-frame velocity components. ϕ, θ, ψ are the conventional roll, pitch, yaw angles of the helicopter fuselage and s_*, c_* denote $\sin(*)$, $\cos(*)$ respectively. It is also critical to point out that the Euler angle derivatives, $\dot{\phi}$, $\dot{\theta}$, $\dot{\psi}$, are not orthogonal to each other. They are related to the body frame angular rates, p, q, r, by the following kinematic equation:

$$\begin{pmatrix}\dot{\phi}\\ \dot{\theta}\\ \dot{\psi}\end{pmatrix} = \begin{bmatrix} 1 & s_\phi s_\theta / c_\theta & c_\phi s_\theta / c_\theta \\ 0 & c_\phi & -s_\phi \\ 0 & s_\phi / c_\theta & c_\phi / c_\theta \end{bmatrix} \begin{pmatrix}p\\ q\\ r\end{pmatrix}. \tag{2}$$

Note that the above equation has singularity at $\theta = 90°$. If full-envelope flight is required, a quaternion representation is recommended in literature. However, since the coaxial helicopter will be flying at near-hover condition for all future missions, it is adequate to use the above equation.

By treating the whole coaxial platform as a rigid mass, the 6 Degrees-of-Freedom (DoF) motion can be described by the Newton-Euler equations:

$$\begin{pmatrix}\dot{u}\\ \dot{v}\\ \dot{w}\end{pmatrix} = \frac{1}{m}\begin{pmatrix}F_x\\ F_y\\ F_z\end{pmatrix} - \begin{pmatrix}p\\ q\\ r\end{pmatrix} \times \begin{pmatrix}u\\ v\\ w\end{pmatrix}, \tag{3}$$

$$\begin{pmatrix}\dot{p}\\ \dot{q}\\ \dot{r}\end{pmatrix} = \mathbf{J}^{-1}\left\{\begin{pmatrix}M_x\\ M_y\\ M_z\end{pmatrix} - \begin{pmatrix}p\\ q\\ r\end{pmatrix} \times \mathbf{J}\begin{pmatrix}p\\ q\\ r\end{pmatrix}\right\}, \tag{4}$$

where F_x, F_y, F_z are projections of the net force, $\mathbf{F}$, onto the body-frame x-, y-, z-axis, and M_x, M_y, M_z are projections of the net torque, $\mathbf{M}$, onto the body-frame x-, y-, z-axis. The compositions of $\mathbf{F}$ and $\mathbf{M}$ come from various parts of the coaxial helicopter and will be explained in detail later. The total mass of the platform, m, can be easily measured, while $\mathbf{J}$ is the moment of inertia of the platform, which is in the form of

$$\mathbf{J} = \begin{bmatrix} J_{xx} & -J_{xy} & -J_{xz} \\ -J_{xy} & J_{yy} & -J_{yz} \\ -J_{xz} & -J_{yz} & J_{zz} \end{bmatrix}.$$

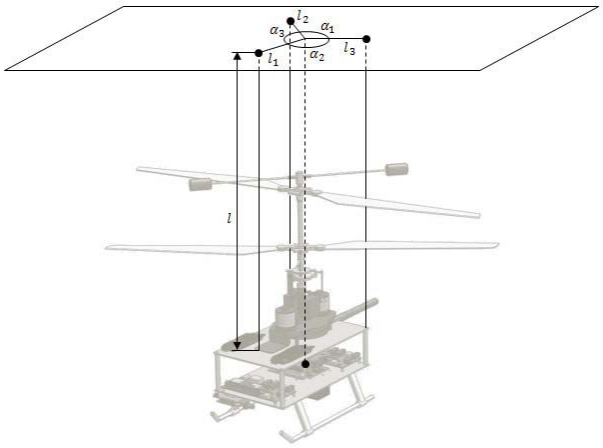

Fig. 4. The trifilar pendulum method

Since the coaxial helicopter being modeled is almost symmetric in both longitudinal and lateral directions, J_{xy}, J_{xz}, J_{yz} are extremely small and can be assumed to be zero. J_{xx}, J_{yy}, J_{zz} can be measured by the trifilar pendulum method proposed in [13]. The experimental setup is shown in Fig. 4. In this experiment, the coaxial platform is suspended by three flexible strings with equal length l. The horizontal distances between the attached points and the CG are l_1, l_2 and l_3 respectively. One can slightly twist and release the platform around the z-axis and record the oscillation period t_l. The moment of inertia is then given by:

$$J_{zz} = \frac{mgl_1l_2l_3t_l^2}{4\pi^2 l} \cdot \frac{l_1 \sin\alpha_1 + l_2 \sin\alpha_2 + l_3 \sin\alpha_3}{l_2l_3 \sin\alpha_1 + l_1l_3 \sin\alpha_2 + l_1l_2 \sin\alpha_3}, \quad (5)$$

where α_1, α_2 and α_3 are the angles denoted in Fig. 4. Similar experiments can be done to obtain the moment of inertia around the other two axes.

B. Force and Torque Composition

As mentioned in the previous sub-section, force and torque acting on the coaxial helicopter come from various mechanical parts. First of all, the helicopter weight exerts a force of mg in the NED-frame z-axis. After converting it to the body frame, the vector is shown as the second term on the right hand side of (6).

Next, when the rotor blades spin, they generate thrusts, $\vec{T}_i$ (i = up, dw) in the direction perpendicular to their respective TPP. When the upper and lower TPPs deviate from their default orientation, the thrust vectors no longer pass through the CG of the helicopter, thus creating rotational torque. The torque vectors caused by the rotor thrusts can be calculated by $\vec{l}_{\text{up}} \times \vec{T}_{\text{up}}$ and $\vec{l}_{\text{dw}} \times \vec{T}_{\text{dw}}$, where $\vec{l}_{\text{up}}$ and $\vec{l}_{\text{dw}}$ are the displacement vectors from helicopter CG to the upper rotor hub and the lower rotor hub respectively. The deviation of the TPP can be described by the longitudinal flapping angle a_i and the lateral flapping angle b_i. The thrust decomposition to the body-frame axes can be approximated by the second equation in (8). Non-zero a_i and b_i also directly result in flapping torque on the rotor hub. This torque can be simplified as the second term on the right hand side of (7), where K_β is the effective spring constant and it has the same value for both the upper and lower rotors.

Furthermore, the rotation of the rotors creates the drag torque, $\vec{Q}_{\text{up}}$ and $\vec{Q}_{\text{dw}}$, around the body-frame z-axis. When the coaxial helicopter hovers without yaw motion, the two torques have the same magnitude, thus canceling each other. Else, if the net drag torque is non-zero, yaw acceleration is generated. In addition, the change of rotational speeds of the rotors also generate the so-called reaction torques on the helicopter body (denoted by $Q_{\text{r,up}}$ and $Q_{\text{r,dw}}$). They are described in (10), where J_{up} and J_{dw} are the moment of inertia of the upper rotor (with stabilizer bar) and the lower rotor with respect to the rotor shaft. They can be calculated by measuring the mass and dimension of the rotor blades and stabilizer bar and assuming a regular geometric shape.

Last but not least, when the helicopter moves in air, its fuselage experiences drag forces, X_{fus}, Y_{fus}, Z_{fus}, due to air resistance. Equation (6) and (7) have summarized all the forces and torques mentioned above, with (8)–(10) explaining how to evaluate the individual terms:

$$\begin{pmatrix} F_x \\ F_y \\ F_z \end{pmatrix} = \sum \vec{T}_i + mg \begin{pmatrix} -s_\theta \\ s_\phi c_\theta \\ c_\phi c_\theta \end{pmatrix} + \begin{pmatrix} X_{fus} \\ Y_{fus} \\ Z_{fus} \end{pmatrix}, \quad (6)$$

$$\begin{pmatrix} M_x \\ M_y \\ M_z \end{pmatrix} = \sum \vec{l}_i \times \vec{T}_i + \sum K_\beta \begin{pmatrix} \sin a_i \\ \sin b_i \\ 0 \end{pmatrix} + \sum \vec{Q}_{\text{d},i} + \sum \vec{Q}_{\text{r},i}\,, \quad (7)$$

$$\vec{l}_i = |\vec{l}_i| \begin{pmatrix} 0 \\ 0 \\ -1 \end{pmatrix}, \quad \vec{T}_i = |\vec{T}_i| \begin{pmatrix} -\sin a_i \\ \sin b_i \\ -\cos a_i \cos b_i \end{pmatrix}, \quad (8)$$

$$\vec{Q}_{\text{d,up}} = |\vec{Q}_{\text{d,up}}| \begin{pmatrix} 0 \\ 0 \\ 1 \end{pmatrix}, \quad \vec{Q}_{\text{d,dw}} = |\vec{Q}_{\text{d,dw}}| \begin{pmatrix} 0 \\ 0 \\ -1 \end{pmatrix}, \quad (9)$$

$$\vec{Q}_{\text{r,up}} = J_{\text{up}}\dot{\Omega}_{\text{up}} \begin{pmatrix} 0 \\ 0 \\ 1 \end{pmatrix}, \quad \vec{Q}_{\text{r,dw}} = J_{\text{dw}}\dot{\Omega}_{\text{dw}} \begin{pmatrix} 0 \\ 0 \\ -1 \end{pmatrix}. \quad (10)$$

C. Thrust and Torque from Rotors

In this sub-section, the magnitude of the rotor thrust and drag torque, $|\vec{T}_i|$ and $|\vec{Q}_{\text{d},i}|$, will be investigated. According to the aerodynamic actuator disk theory [14], the magnitude of thrust generated by the rotors can be formulated as follows:

$$|\vec{T}_i| = \rho C_{T,i} A (\Omega_i R)^2, \quad (11)$$

where ρ is the density of air, $C_{T,i}$ is the lift coefficient, A is the rotor disk area, Ω_i is the rotational speed of the rotor and R is the rotor blade length. Since this is a fixed-pitch coaxial helicopter, $C_{T,i}$, like the other parameters in (11), is constant. The only variable is Ω_i. Hence, the equation can be simplified to:

$$|\vec{T}_i| = k_{T,i} \Omega_i^2, \quad (12)$$

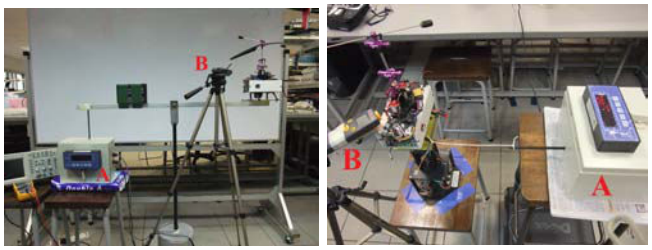

Fig. 5. Setup to investigate relation between thrust / torque and rotor speed

where $k_{T,i}$ is an overall thrust coefficient that needs to be identified. Similar assumptions and formulation can be applied to the relationship between the drag torque and the rotational speed of the rotors:

$$|\vec{Q}_{\mathrm{d},i}| = k_{Q,i}\Omega_i^2. \tag{13}$$

To identify $k_{T,i}$ and $k_{Q,i}$, two test bench experiments were carried out (see Fig. 5). The main measurement sensors include a force meter (A) and a tachometer (B). For the thrust experiment, results are summarized in Fig. 6. There are four lines in the plot, in which two of them (solid lines) perfectly match. They represent the cases when only one rotor (upper rotor or lower rotor) is rotating. The dashed line on the top is a numerical combination of the two solid lines, while the dash-dot line comes from actual tests with both rotors spinning at approximately the same speed. The gap between the two lines shows a drop in thrust efficiency caused by aerodynamic interactions between the two rotors. According to [15], for a coaxial helicopter operating in near-hover condition, the induced-velocity effect of the upper rotor to the lower rotor is significantly larger than that of the lower rotor to the upper rotor. Thus, the loss of thrust efficiency can be fully accounted on the lower rotor thrust coefficient. Hence, $k_{T,\mathrm{up}}$ is the gradient of the solid line and $k_{T,\mathrm{dw}}$ is the gradient difference between the dash-dot line and the solid line.

For the torque experiment, results are summarized in Fig. 7. The solid line represents the case when only the stabilizer bar is rotating, while the dash-dot line is for a single rotating rotor. The dashed line is generated with the upper rotor and the stabilizer bar spinning together. Unsurprisingly, it matches the numerical combination of the lower two lines. Thus, the gradient of the dashed line is $k_{Q,\mathrm{up}}$, and the gradient of the dash-dot line is $k_{Q,\mathrm{dw}}$.

D. Rotor Tip-Path-Plane Motion

For this type of coaxial helicopter, the rotor collective pitch is fixed. But its cyclic pitch can change. For the lower rotor, the rotor hub is connected to the aileron and the elevator servos via a swashplate. When the swashplate tilts, it teeters the rotor hub and creates a cyclic pitch on the rotor. For every cycle of rotation, the rotor blade will reach the maximum angle of attack at a particular phase angle at which the lift on the blade is largest. This results in the flapping of the rotor disk. The whole mechanism is a combination of gyroscopic precession and aerodynamic precession. For the

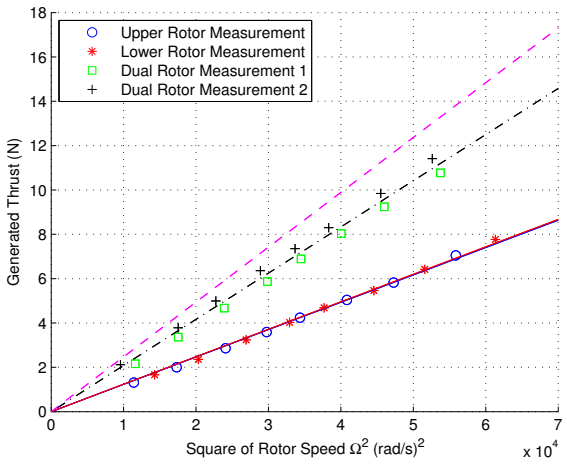

Fig. 6. Data plot of thrust against square of rotor speed

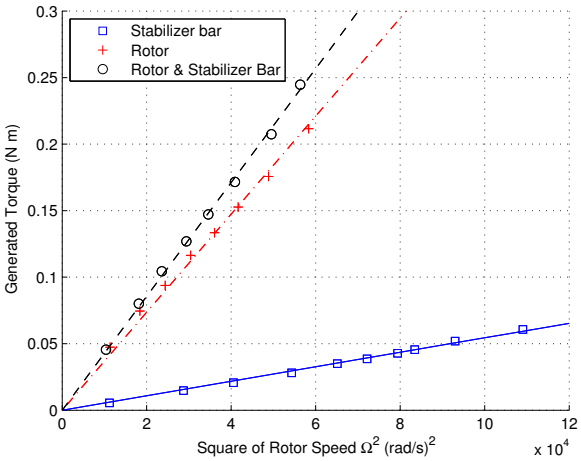

Fig. 7. Data plot of torque against square of rotor speed

case of FeiLion, if one observes the rotor blade in a slow motion, the maximum rotor flapping occurs roughly at 45° lag with respect to the occurrence of maximum angle of attack. This explains why the aileron and elevator servos of the off-the-shelf coaxial platform are connected to the swashplate 45° off the body-frame x-, y-axis. In this way, the aileron servo mainly controls the lateral flapping of the lower rotor, and the elevator servo mainly controls the longitudinal flapping. However, the flapping phase lag is not exactly equal to 45° (slightly larger than 45° from test bench observations) due to mechanical modifications to the original RC platform (original rotor blades have been replaced by stiffer ones for larger payload). This results in non-negligible coupling between the servo inputs and the lower rotor longitudinal and lateral flapping angles. As the lower rotor does not have any additional damping mechanism attached, its flapping process is almost instantaneous. By assuming a first order dynamics, the time constant can be observed via a high-speed camera. The result turns out to be 0.0375 second, which is very small as compared to dynamics happening in other parts of the coaxial helicopter, thus can be neglected. Hence, the

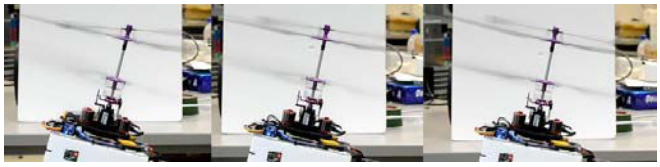

Fig. 8. Step response of stabilizer bar TPP motion (Left: $t = 0$; Middle: $t = 0.2$ s; Right: $t = \infty$)

relationship between servo inputs and lower rotor flapping angles can be formulated in a simple non-dynamic way:

$$a_{\text{dw}} = A_{a,\text{dw}}\,\delta_{\text{ele}} + A_{b,\text{dw}}\,\delta_{\text{ail}} - A_q\,q, \tag{14}$$

$$b_{\text{dw}} = B_{b,\text{dw}}\,\delta_{\text{ail}} + B_{a,\text{dw}}\,\delta_{\text{ele}} - B_p\,p, \tag{15}$$

where δ_{ail}, δ_{ele} are the servo inputs normalized to [-1, 1], $A_{a,\text{dw}}$ and $B_{b,\text{dw}}$ are the on-axis steady-state ratio from servo inputs to flapping angles, and $A_{b,\text{dw}}$ and $B_{a,\text{dw}}$ are the off-axis (coupling) values. The terms depending on angular rates, p and q, come from an effect called rotor damping, which was also considered in [16] but in a quadratic form.

For the upper rotor system, a stabilizer bar is attached to the rotor hub, so that they teeter together. As the stabilizer bar has large moment of inertia, it tends to remain at its original rotating plane. Hence, at the moment when the helicopter body tilts, the stabilizer bar TPP will remain at the level plane, thus creating a cyclic pitch on the upper rotor which leads to blade flapping. The torque generated by this flapping redresses the rotational motion of the helicopter and significantly stabilizes the whole platform attitude. Similar to the lower rotor system, the stabilizer bar is installed at 45° phase lead to the rotor blade. In this way, the maximum flapping happens at the direction that roughly counters the rotational motion of the helicopter. Again, there is coupling between the longitudinal and lateral channels because the flapping phase lag is not exactly 45°. The following equations describe the above-mentioned dynamics:

$$\dot{\phi}_{\text{sb}} = \frac{1}{\tau_{\text{sb}}}\,(\phi - \phi_{\text{sb}}), \tag{16}$$

$$\dot{\theta}_{\text{sb}} = \frac{1}{\tau_{\text{sb}}}\,(\theta - \theta_{\text{sb}}), \tag{17}$$

$$a_{\text{up}} = A_{a,\text{up}}\,(\theta_{\text{sb}} - \theta) + A_{b,\text{up}}\,(\phi_{\text{sb}} - \phi) - A_q\,q, \tag{18}$$

$$b_{\text{up}} = B_{b,\text{up}}\,(\phi_{\text{sb}} - \phi) + B_{a,\text{up}}\,(\theta_{\text{sb}} - \theta) - B_p\,p, \tag{19}$$

where ϕ_{sb} and θ_{sb} are the roll and pitch angles of the stabilizer bar TPP, $A_{a,\text{up}}$ and $B_{b,\text{up}}$ are the on-axis steady-state ratio from the stabilizer bar teetering angles to the upper rotor flapping angles, and $A_{b,\text{up}}$ and $B_{a,\text{up}}$ are the off-axis (coupling) values. Again, the same rotor damping effects (terms depending on p and q) are considered for the upper rotor flapping dynamics.

For the identification of τ_{sb}, one can observe the transient step response of the stabilizer bar TPP (see Fig. 8) by a high-speed camera and record the time when the response reaches 63.1% of the overall amplitude. On-axis parameters $A_{a,\text{up}}$, $B_{b,\text{up}}$, $A_{a,\text{dw}}$ and $B_{b,\text{dw}}$ can be identified by measuring various angles (see Fig. 9 and Fig. 10) and assuming a linear relationship between each pair of them. For the other coupling values and K_β, they can be identified by analyzing flight test data with aileron and elevator channel perturbations (frequency sweeping). The software used for numerical analysis is named 'Comprehensive Identification from FrEqency Responses' (CIFER). It is a MATLAB-based software developed by NASA Ames Research Center for military based rotorcraft system identifications. By combining and linearizing all the aforementioned equations related to angular rate dynamics and upper rotor flapping dynamics, one can obtain the following linear state-space approximation:

$$\begin{bmatrix} \dot{p} \\ \dot{q} \\ \dot{a}_{\text{up}} \\ \dot{b}_{\text{up}} \end{bmatrix} = \begin{bmatrix} \frac{-X_{\text{dw}}B_{p,\text{dw}}}{J_{xx}} & 0 & 0 & \frac{X_{\text{up}}}{J_{xx}} \\ 0 & \frac{-X_{\text{dw}}A_{q,\text{dw}}}{J_{yy}} & \frac{X_{\text{up}}}{J_{yy}} & 0 \\ -A_{b,\text{up}} & -A_{a,\text{up}} & -\frac{1}{\tau_{\text{sb}}} & 0 \\ -B_{b,\text{up}} & -B_{a,\text{up}} & 0 & -\frac{1}{\tau_{\text{sb}}} \end{bmatrix} \begin{bmatrix} p \\ q \\ a_{\text{up}} \\ b_{\text{up}} \end{bmatrix} + \begin{bmatrix} \frac{X_{\text{dw}}B_{b,\text{dw}}}{J_{xx}} & \frac{X_{\text{dw}}B_{a,\text{dw}}}{J_{xx}} \\ \frac{X_{\text{dw}}A_{b,\text{dw}}}{J_{yy}} & \frac{X_{\text{dw}}A_{a,\text{dw}}}{J_{yy}} \\ 0 & 0 \\ 0 & 0 \end{bmatrix} \begin{bmatrix} \delta_{\text{ail}} \\ \delta_{\text{ele}} \end{bmatrix}, \tag{20}$$

where $X_{\text{up}} = T_{\text{up}}l_{\text{up}} + K_\beta$ and $X_{\text{dw}} = T_{\text{dw}}l_{\text{dw}} + K_\beta$. By treating δ_{ail}, δ_{ele} as the inputs and p, q as the outputs (all can be recorded during flight tests) and giving known constraints and reasonable initial values, CIFER helps to search for optimal numerical solution based on frequency response matching. A stable result with good matching is obtained as follows:

$$\begin{bmatrix} \dot{p} \\ \dot{q} \\ \dot{a}_{\text{up}} \\ \dot{b}_{\text{up}} \end{bmatrix} = \begin{bmatrix} -17.19 & 0 & 0 & 934.1 \\ 0 & -5.360 & 291.3 & 0 \\ 0.2745 & -0.49 & -5 & 0 \\ -0.49 & -0.2745 & 0 & -5 \end{bmatrix} \begin{bmatrix} p \\ q \\ a_{\text{up}} \\ b_{\text{up}} \end{bmatrix} + \begin{bmatrix} -102.48 & -38.08 \\ -11.73 & 31.95 \\ 0 & 0 \\ 0 & 0 \end{bmatrix} \begin{bmatrix} \delta_{\text{ail}} \\ \delta_{\text{ele}} \end{bmatrix}, \tag{21}$$

By comparing (20) and (21), all the remaining parameters involved in angular rate and rotor flapping dynamics can be identified.

E. Fuselage Drag

When the helicopter fuselage moves in air, it experiences drag force acting on the opposite direction of the motion. For the body-frame horizontal directions, the rotor downwash is deflected by u and v. In the situation when u (or v) is less than v_i (the induced velocity of air at the lower rotor), the downwash effect needs to be taken into account. Otherwise, the downwash effect is relatively weak and can be ignored. The fuselage in all three directions are considered as a flat plate perpendicular to the helicopter motion, thus the drag

Fig. 9. Left: Maximum teetering angle of the lower rotor hub; Right: Maximum flapping angle of the lower rotor

Fig. 10. Left: Maximum teetering angle of the stabilizer bar; Right: Maximum teetering angle of the upper rotor hub

coefficient is approximately unity. As such, the horizontal fuselage drag forces are formulated in a quadratic form:

$$X_{\text{fus}} = -\frac{\rho}{2} S_x u \cdot \max(v_i, |u|), \tag{22}$$

$$Y_{\text{fus}} = -\frac{\rho}{2} S_y v \cdot \max(v_i, |v|), \tag{23}$$

$$v_i = \sqrt{\frac{|T_{dw}|}{2\rho\pi R^2}}, \tag{24}$$

where S_x and S_y are the effective drag area along the body-frame x- and y-axis respectively.

For the vertical direction, since the fuselage is constantly exposed to the lower rotor downwash, it is commonly formulated in the following form:

$$Z_{\text{fus}} = -\frac{\rho}{2} S_z (w - v_i)|w - v_i|. \tag{25}$$

However, as the lift coefficient test for identifying $k_{T,i}$ in (12) was done with the presence of the fuselage (so the term $\frac{\rho}{2} S_z v_i^2$ has already been taken into account), the above equation needs to be compensated as:

$$Z_{\text{fus}} = -\frac{\rho}{2} S_z w \cdot \max(v_i, |w|), \tag{26}$$

where S_z is the effective drag area along the body-frame z-axis.

In this sub-section, parameters to be identified are ρ, R, S_x, S_y and S_z. All of them can be easily obtained by direct measurement.

F. Motor Speed Dynamics

Two brushless DC motors are used on FeiLion. Their rotational speed dynamics follows the well-known differential equation of electro motors:

$$J_{\text{mot}}\dot{\omega} = \frac{k_{\text{m}} U - k_{\text{m}} k_{\text{e}} \omega}{R_{\text{mot}}} - d\omega - M_{\text{L}}, \tag{27}$$

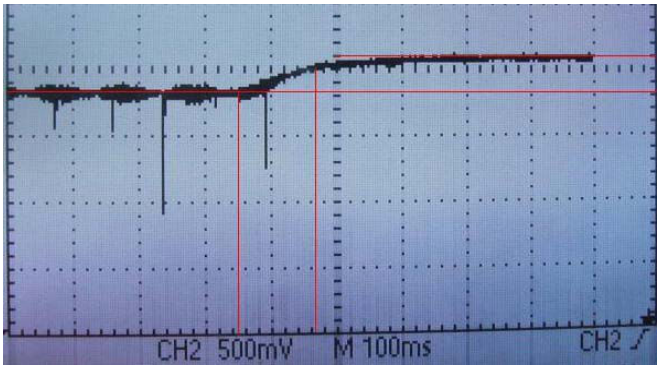

Fig. 11. Estimation of time constant of motor speed dynamics

where J_{mot} is the motor moment of inertia, k_{m} and k_{e} are the mechanical and electrical motor constants, U is the input voltage, R_{mot} is the resistance of the circuit, d is the friction coefficient, and M_{L} is the external torque acting on the motor shaft. Here, M_{L} is equal to the rotor drag torque $Q_{\text{d},i}$ appeared in (13). If the helicopter operates at a near-hover condition, everything can be approximated linearly. M_{L} can be assumed to be a combination of a constant trimming value, M_{L}^*, and another term proportional to extra rotational speed as compared to the trimming speed, Ω^*:

$$M_{\text{L}} = M_{\text{L}}^* + k_{\text{L}}(\Omega - \Omega^*). \tag{28}$$

Further considering that the rotational speed of rotor, Ω, and the rotational speed of the motor, ω, are perfectly proportional by the gear ratio, the rotor speed dynamics can be simplified to the following first-order equations:

$$\dot{\Omega}_{\text{up}} = \frac{1}{\tau_{\text{mt}}}(m_{\text{up}}\delta_{\text{up}} + \Omega_{\text{up}}^* - \Omega_{\text{up}}), \tag{29}$$

$$\dot{\Omega}_{\text{dw}} = \frac{1}{\tau_{\text{mt}}}(m_{\text{dw}}\delta_{\text{dw}} + \Omega_{\text{dw}}^* - \Omega_{\text{dw}}), \tag{30}$$

where Ω_{up}^* and Ω_{dw}^* are the trimming values of the rotor rotational speed at hovering, τ_{mt} is the time constant of the motor speed dynamics, and m_{up}, m_{dw} are the steady-state ratio between the change of rotor speeds and the change of motor inputs.

The identification of τ_{mt} is rather indirect. Instead of examining the transient response of the rotor speed with motor step input, which is very difficult to be carried out, the transient response of the input voltage subject to the changes of the motor Back-EMF (voltage generated by the spinning motor) is recorded using an oscilloscope (see Fig. 11). The time constant of the the two transient response should be the same. m_{up} and m_{dw} can be identified by plotting the steady-state relationship between the rotor speed and the motor input (see Fig. 12). m_{up} and m_{dw} are the gradients of the two fitted lines in the figure.

G. Mixer and Headlock Gyro Dynamics

In order to decouple the throttle-heave and the rudder-yaw dynamics, the throttle and rudder signals are passed into a hardware mixer and transformed to dual motor control

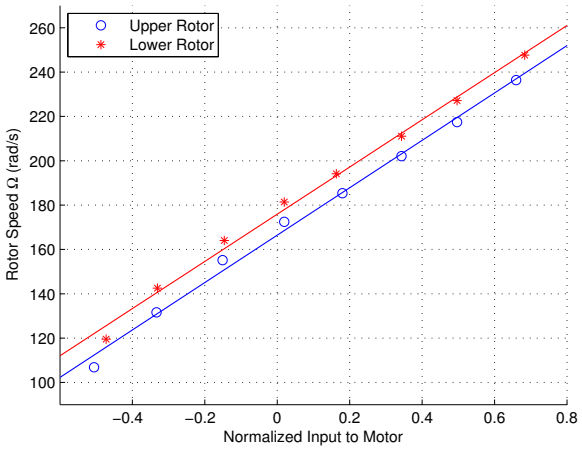

Fig. 12. Data plot of rotor speed against motor input

TABLE I

YAW RATE AGAINST RUDDER INPUT: HOVERING TURN

r (rad/s)	−1.50	−2.50	−2.60	−3.50
δ_{rud} $(-1, 1)$	0.25	0.35	0.40	0.55

TABLE II

IDENTIFIED PARAMETERS (IN SI UNITS)

$\rho = 1.204$ $m = 0.977$ $R = 0.250$ $g = 9.781$	$m_{\text{up}} = 106.90$ $m_{\text{dw}} = 106.45$ $\tau_{\text{sb}} = 0.2$ $\tau_{\text{mt}} = 0.12$	$\Omega^*_{\text{up}} = 203.38$ $\Omega^*_{\text{dw}} = 217.88$ $K_\beta = 4.377$
$S_{fx} = 0.00835$ $S_{fy} = 0.01310$ $S_{fz} = 0.01700$	$K_{\text{a}} = 6.4267$ $K_{\text{P}} = 0.667/K_{\text{a}}$ $K_{\text{I}} = 0.713/K_{\text{a}}$	$J_{xx} = 0.0059$ $J_{yy} = 0.0187$ $J_{zz} = 0.0030$
$l_{up} = 0.195$ $l_{dw} = 0.120$	$J_{\text{up}} = 6.8613 \cdot 10^{-4}$ $J_{\text{dw}} = 3.2906 \cdot 10^{-4}$	$A_q = 0.0204$ $B_p = 0.0204$
$k_{T,\text{up}} = 1.23 \cdot 10^{-4}$ $k_{T,\text{dw}} = 8.50 \cdot 10^{-5}$ $k_{Q,\text{up}} = 4.23 \cdot 10^{-6}$ $k_{Q,\text{dw}} = 3.68 \cdot 10^{-6}$	$A_{a,\text{up}} = 0.4900$ $A_{b,\text{up}} = -0.2745$ $B_{a,\text{up}} = 0.2745$ $B_{b,\text{up}} = 0.4900$	$A_{a,\text{dw}} = 0.1217$ $A_{b,\text{dw}} = -0.0450$ $B_{a,\text{dw}} = -0.0450$ $B_{b,\text{dw}} = -0.1217$

signals:

$$\delta_{up} = \delta_{\text{thr}} + \bar{\delta}_{\text{rud}}, \quad (31)$$

$$\delta_{dw} = \delta_{\text{thr}} - \bar{\delta}_{\text{rud}}. \quad (32)$$

One can clearly see that when the throttle signal δ_{thr} increases, inputs to both motors increase; when the rudder signal $\bar{\delta}_{\text{rud}}$ increases, the input to the motor connected to the upper rotor increases while the input to the motor connected to the lower rotor decreases.

Note that the rudder signal in the above mixer equation is not the original signal δ_{rud}. From δ_{rud} to $\bar{\delta}_{\text{rud}}$, there is a hardware headlock gyro which helps refine the rudder signal and acts as a most inner-loop yaw motion stabilizer. Usually, there is a P-I controller embedded inside the headlock gyro and it can be formulated as follows:

$$\dot{r}_{\text{fb}} = K_{\text{a}}\delta_{\text{rud}} - r, \quad (33)$$

$$\bar{\delta}_{\text{rud}} = K_{\text{P}}(K_{\text{a}}\delta_{\text{rud}} - r) + K_{\text{I}} r_{\text{fb}}, \quad (34)$$

where r_{fb} is the augmented state needed by the integral control. K_{a} can be identified by performing manual hovering turn of the helicopter with rudder input at different values. The recorded data is shown in Table I (steady-state values). The linear gradient of yaw rate against rudder input equals to the value of K_{a}. Next, by placing the helicopter stationary on a test bench, K_{P} and K_{I} can be identified by observing the headlock gyro output signal (in Pulse Width Modulation form) caused by a small known step inputs. The initial ratio between the output and the input is $K_{\text{P}}/K_{\text{a}}$, while the climbing rate of the step response is $K_{\text{I}}/K_{\text{a}}$. At this point, the full dynamics of a coaxial helicopter have been mathematically formulated and all important model parameters have been identified. Table II has listed all the identified parameters for FeiLion.

IV. MODEL VERIFICATION

In this section, a comprehensive evaluation on the fidelity of the obtained nonlinear model is shown. Four manual flight tests were carried out, which include:

1) Aileron channel perturbation with FeiLion rolling left and right,
2) Elevator channel perturbation with FeiLion pitching forward and backward,
3) Throttle channel perturbation with FeiLion flying up and down,
4) Rudder channel perturbation with FeiLion yawing clockwise and anticlockwise.

In these four flight tests, the pilot was asked to try his best to agitate only one of the four input channels. However, to make sure the helicopter position does not drift too much (safety needs to be ensured), minor off-axis inputs were also issued to lightly counter the cross-couplings between the channels. The time-domain results are shown in Fig. 13–16. Based on the recorded inputs, the transient response of the UAV attitudes, angular rates and body-frame velocities are calculated by a MATLAB simulation program with the aforementioned nonlinear mathematical model (dashed lines in the figures). They are plotted together with the in-flight true data obtained by the onboard sensors (solid lines in the figures). The matching between the two is quite promising. Note that for angular rate dynamics, both the on-axis response and off-axis response matches well. Some minor mismatches are caused by the ignorance of high frequency dynamics when formulating the model, especially for the motion of rotor flapping, which is highly complicated. Other discrepancies come from ground effect (wind disturbances) and measurement noises present in practical flight tests. In general, this is an accurate cross-coupled model for a fixed-pitch coaxial UAV with low maneuvering speed.

V. CONCLUSIONS AND FUTURE WORKS

In conclusion, the nonlinear model of a fixed-pitch coaxial UAV, FeiLion, is fully derived. The model formulation starts from the 6-DoF rigid body dynamics. Forces and torques from various mechanical parts of the helicopter are analyzed. Sub-systems including rotor thrust-torque generation, rotor

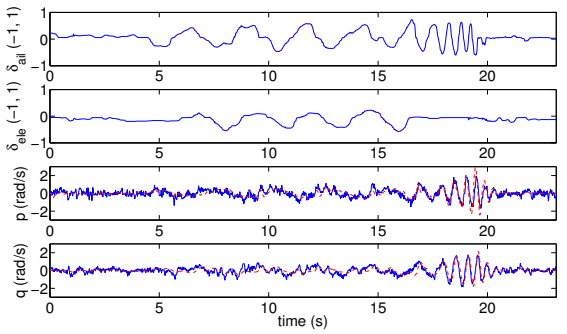

Fig. 13. Responses from aileron input perturbation

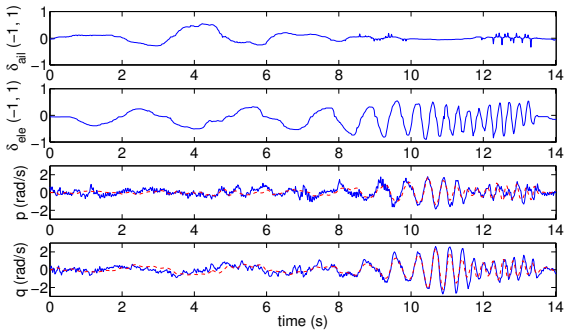

Fig. 14. Responses from elevator input perturbation

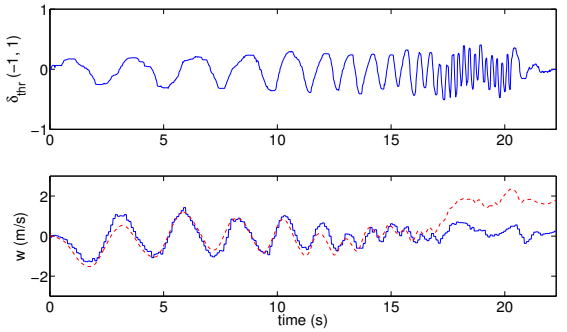

Fig. 15. Responses from throttle input perturbation

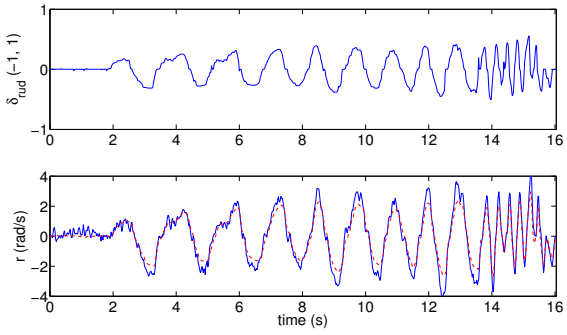

Fig. 16. Responses from rudder input perturbation

TPP dynamics, fuselage drag, motor speed dynamics, mixer and headlock gyro dynamics are discussed in detail. For each of them, methods of obtaining the model parameters are described and the corresponding test results are shown. The derived model is also verified by conducting actual flight tests and comparing simulation results with the in-flight sensor measurements. Good matching between the two has proven the model fidelity. In the near future, this model will be used to design high-performance robust controllers such as LQG or H_∞ on FeiLion. After it is well stabilized in autonomous flight tests, indoor navigation strategy based on sensors like camera and scanning laser range finder will be implemented in the next stage.

REFERENCES

[1] P. Mukherjee and S. L. Waslander, "Modeling and Multivariable Control Techniques for Small Coaxial Helicopters," *AIAA Guidance, Navigation, and Control Conference*, 2011, AIAA-2011-6545.

[2] C. Coleman, "A Survey of Theoretical and Experimental Coaxial Rotor Aerodynamic Research," Tech. Rep. 3675, NASA Ames Research Center, 1997.

[3] L. Chen and P. McKerrow, "Modelling the Lama Coaxial Helicopter," *Proceedings of the Australasian Conference on Robotics and Automation*, 2007, pp. 1-7.

[4] B.Mettler, *Identification Modeling and Characteristics of Miniature Rotorcraft*, Kluwer Academic Publishers, 2003.

[5] G. Cai, B. M. Chen, T. H. Lee and K. Y. Lum, "Comprehensive Nonlinear Modeling of an Unmanned-Aerial-Vehicle Helicopter," *AIAA Guidance, Navigation and Control Conference and Exhibit*, 2008, AIAA-2008-7414.

[6] O. Rand and V. Khromov, "Aerodynamic Optimization of Coaxial Rotor in Hover and Axial Flight," *27th international Congress of the Aeronautical Sciences*, 2010, pp. 1-13.

[7] H. W. Kim and R. E. Brown, "Coaxial Rotor Performance and Wake Dynamics in Steady and Manoeuvring Flight," *American Helicopter Society 62nd Annual Forum Proceedings*, vol. 1, 2006, pp. 20-40.

[8] D. Schafroth, C. Bermes, S. Bouabdallah and R. Siegwart, "Modeling and System Identification of the muFly Micro Helicopter," it Journal of Intelligent and Robotic Systems, vol. 57, no. 1-4, 2010, pp. 27-47.

[9] D. Neamtu, R. Deac, R. D. Keyser, C. Ionescu and I. Nascu, "Identification and Control of a Miniature Rotorcraft Unmanned Aerial Vehicle (UAV)," *AQTR'10 Proceedings of the IEEE International Conference on Automation, Quality and Testing, Robotics*, 2010, pp. 1-6.

[10] F. Wang, T. Wang, B. M. Chen and T. H. Lee, "An Indoor Unmanned Coaxial Rotorcraft System with Vision Positioining," *8th IEEE International Conference on Control and Automation*, 2010, pp. 291-296.

[11] S. K. Phang, J. J. Ong, R. T. C. Yeo, B. M. Chen and T. H. Lee, "Autonomous Mini-UAV for indoor flight with embedded on-board vision processing as navigation system," *Computational Technologies in Electrical and Electronics Engineering (SIBIRCON), 2010 IEEE Region 8 International Conference on Digital Object Identifier*, 2010, pp. 722-727.

[12] F. Wang, S. K. Phang, J. Cui, B. M. Chen and T. H. Lee, "Search and Rescue: a UAV Aiding Approach," *23rd Canadian Congress of Applied Mechanics*, 2011, pp. 183-186.

[13] C. M. Harris, *Shock and Vibration Handbook*, 4th ed. New York, NY:McGraw-Hill, 1996.

[14] A. R. S. Bramwell, G. Done and D. Balmford, *Bramwell's Helicopter Dynamics*, Oxford, England: Butterworth-Heinemann, 2nd ed., 2001.

[15] Y. Deng, R. Tao and J. Hu, "Experimental Investigation of the Aerodynamic Interaction Between Upper and Lower Rotors of a Coaxial Helicopter," *ACTA Aeronautica ET Astronautica Sinica*, vol. 24, no. 1, 2003, pp. 10-14.

[16] P. Fankhauser, S. Bouabdallah, S. Leutenegger and R. Siegwart "Modeling and Decoupling Control of the CoaX Micro Helicopter," *2011 IEEE/RSJ International Conference on Intelligent Robots and Systems*, San Francisco, CA, USA, 2011, pp. 25-30.